Stratified surface layers on rails

Messaadi, Maha; Steenbergen, Michaël

DOI
10.1016/j.wear.2018.07.019

Publication date
2018

Document Version
Accepted author manuscript

Published in
Wear

Stratified Surface Layers on Rails

Maha Messaadi, Michaël Steenbergen*

Delft University of Technology, Section of Railway Engineering, Faculty of Civil Engineering and Geosciences, Stevinweg 1, 2628 CN Delft, The Netherlands

Abstract

This study examines the properties of stratified surface layers on rails in service and presents a hypothesis explaining their origin. The stratified layer consists of a white etching top layer and a brown sublayer. The metallurgical composition and properties of this sublayer are found to match with that of globular bainite. The occurrence of stratification in the surface layer is explained by the thermomechanical cycle for a material point on the rail surface under wheel-rail contact. Difference in the surface and subsurface cooling rates after reaching the austenitisation temperature may lead, depending on the chemical steel composition, to the generation of two different phases (martensite and bainite) and stratification. The exclusive occurrence of sandwich layers on rails that have been in service is attributed to the hardening of the top layer, leading to a reduced thermal conductivity, which gains relevance at an increasing depth. The granular morphology of the bainitic sublayer, exhibiting weak globular inclusions, facilitates the initiation and the propagation of transverse cracks, thus contributing to the development of RCF.

Keywords: White etching layer (WEL), brown etching layer (BEL), stratified surface layer, thermomechanical cycle, granular bainite, rolling contact fatigue (RCF).

1. Introduction

*Corresponding author.
E-mail address: M.J.M.M.Steenbergen@tudelft.nl (M. Steenbergen)

Although white etching layers (WEL) on rails are a well-known phenomenon for many decades and associated to profile wear, a WEL or the presence of discrete portions of white etching material on the surface of pearlitic rails are increasingly considered as a preliminary form of damage; their presence is related to the initiation of rolling contact fatigue (RCF) for rails exhibiting insufficient natural wear [1–3]. The WEL can be defined as a tribologically transformed layer which is the result of mechanical and/or thermal wheel-rail interaction in the contact zone [4]. Sometimes however, the layer shows stratification [5], leading to an internal sandwich structure. In this framework, recent work [6] raised the question whether, apart from the 'classical' WEL, also a phase denoted as 'brown etching layer' (BEL) may contribute to RCF development. This brown etching layer is found as a sublayer in stratified surface layers; it is named after the brown color that appears in optical microscopy after etching with a Nital agent. The brown etching layer is found exclusively in coexistence with the white etching surface layer, and according to the experience of the authors, it is found exclusively in samples taken from rails that have been in service. Eventual white surface layers on new rails or rails that have been subject to some kind of surface finishing such as grinding or milling do not show any stratification [4].

In spite of efforts to simulate the formation of transformed surface layers experimentally [7, 8], no explanation has yet been given for the alternation between white and brown phases at the rail surface. In the literature, apart from the previously discussed work, stratified surface layers have been discussed in relation to train wheels, where stratification in thermally transformed layers of considerable thickness (order 1 mm) was caused by multiple skidding, with exposition times in the order of seconds (or even tens of seconds) [9]. Both distinct sublayers in this case are white etching, and the stratification was explained by tempering of previously generated martensite at the surface, giving rise to the presence of primary martensite in the subsurface and secondary martensite at the surface. The BEL considered in this study has different features, is typically formed in the absence of any macroslip and is present over larger lengths of rail, with local flash temperatures (as will be discussed later in this paper) with a duration in the order of milliseconds and having a different order of thickness magnitude (order 10 µm).

Fig. 1 shows examples of a stratified WEL on rail grades R260Mn (standard) and R350HT (heat-treated) with a clear sandwich structure. All samples are taken from a rail in service, with mixed passenger and freight train operation. In all cases shown in Fig. 1, a distinct relatively dark layer, referred to in this paper as brown phase or

BEL, can be observed between the white top layer and the pearlitic matrix of the parent material. Experience shows (see Fig. 1e) that this brown phase can also reach the free surface and be present over a certain length there, but typically it never occurs individually - without any white phase at all. Moreover, in many cases a color gradient can be observed within the brown sublayer, with the darkest color close to the interface with the white layer.

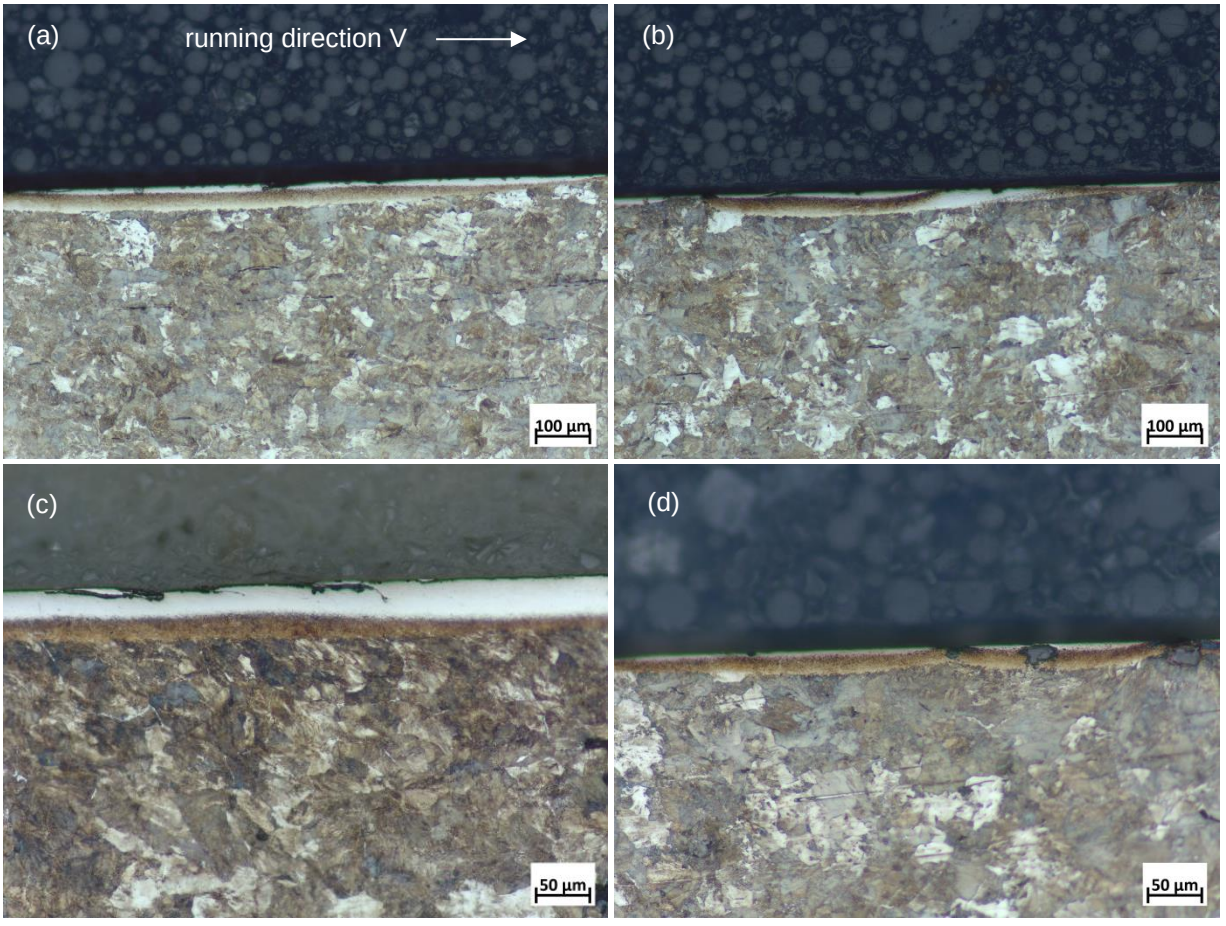

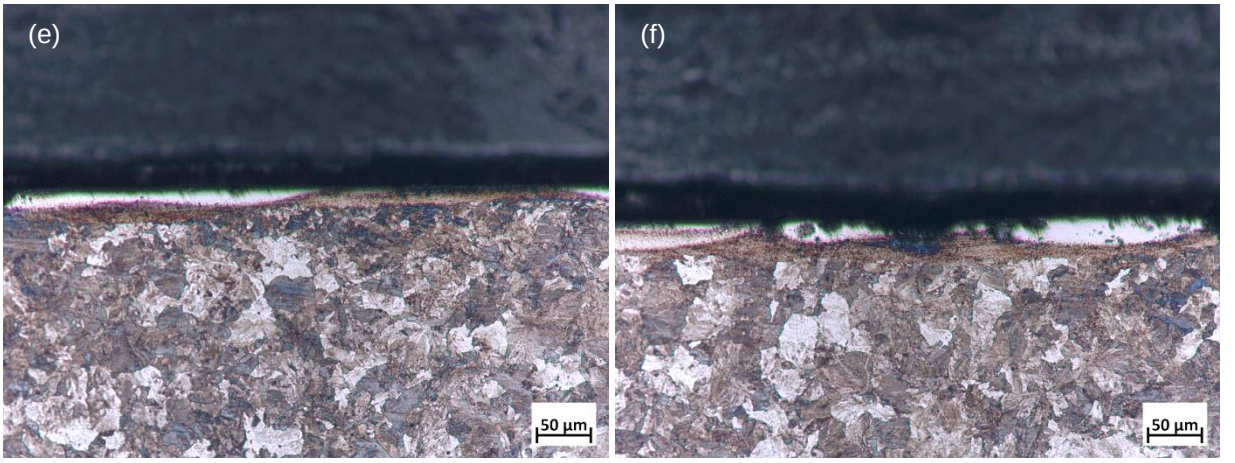

Fig. 1. Appearance of stratified surface layers on rail grades R260Mn (longitudinal section) (a-d) and R350HT (transverse section) (e,f) after 2% Nital etching under optical microscopy.

The phenomenon of stratification of the rail surface layer has been covered only marginally in the literature, addressing the phenomenon as such; its metallurgical nature and origin remain unknown. Therefore, this study addresses the stratification of white etching (or: partially white etching) surface layers following two objectives:

i. determining the internal morphology and the metallurgical nature or phase of the brown etching material;
ii. clarifying its formation by proposing a scenario based on thermomechanical wheel-rail interaction, in line with the findings of the first objective.

The structure of this work is as follows. Section 2 examines the stratification structure at the rail surface in detail. Section 3 proceeds with a metallurgical identification of the brown etching sublayer. In section 4, a hypothesis, in line with the findings of the previous sections, is presented and discussed. This hypothesis incorporates both metallurgical and thermomechanical aspects of wheel-rail contact. Section 5 examines the role of the stratified surface layer in relation to RCF, establishing specific failure modes. Section 6 closes with conclusions.

2. The stratified surface layer: phenomenology & discussion

The structure of the stratified surface layer is analyzed, for the sample shown in Fig. 1a-b, both by optical microscopy (OM) and scanning electron microscopy (SEM); the latter to study in more detail the morphology of the individual sublayers and their interfaces. The results are shown in Fig. 2, from which it can be observed that

each layer has a clearly distinct morphology. It is remarkable that the SEM image shows a smaller thickness for the white top layer as compared to OM, for which technique the interfaces are quite diffuse.

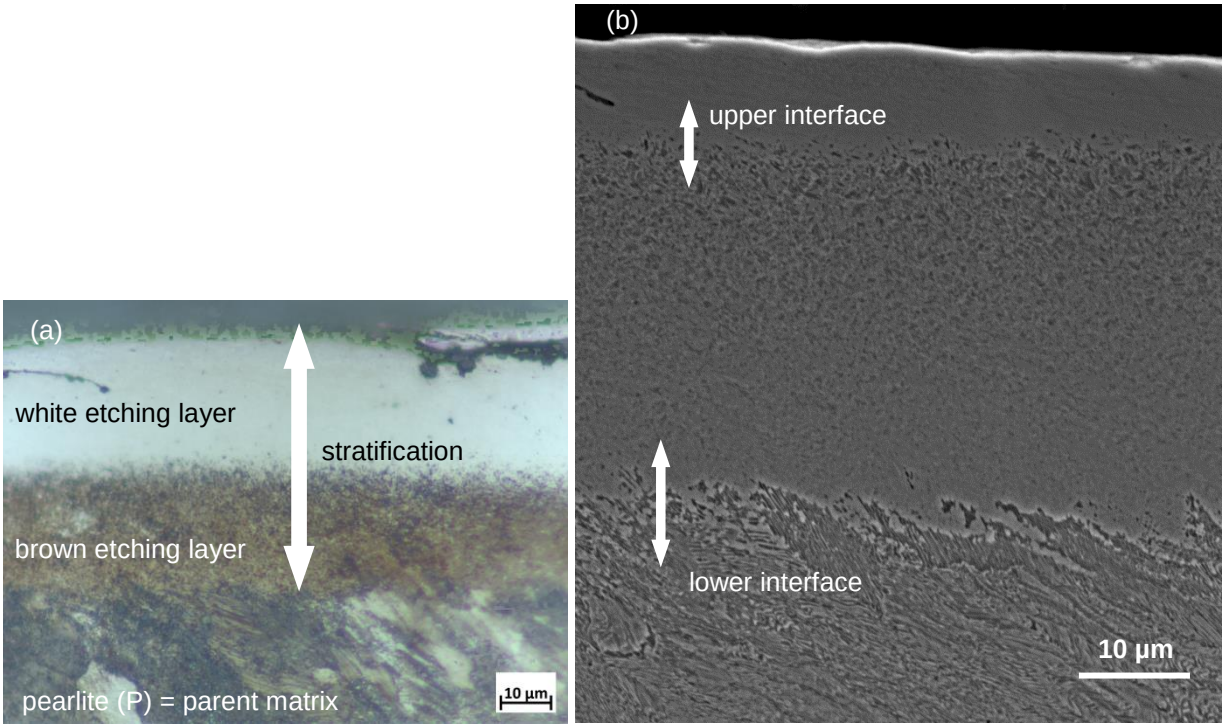

Fig. 2. Structure of stratified layers, (a) optical microscopy (OM), (b) Scanning electron microscopy (SEM).

A number of studies in the scientific literature are devoted to the question of the origin of the WEL in general, discussing thermal or mechanical possibilities [8]. The literature is concurrent in its view that the phase of the WEL is martensitic when a clear granular structure is still present inside this layer [5, 9, 10]. In the case of a mechanical origin, the WEL is found to be a nanostructured layer with extreme hardness (typically exceeding 1000 HV) as compared to the parent material [11]. In contrast to such nanostructured layers, thermally formed layers generally exhibit the following features:

- an absence of plasticity in the subsurface, and especially at the interface between WEL and parent material;
- a similar phase morphology as compared to thermal martensite with twin and lath structure;
- hardness values typically comparable to that of martensite (in the order of 700 HV), which is much lower as compared to the nanostructure hardness.

Observation of the stratified layer as such, taking into account these ‘criteria’, would suggest a thermal origin.

Fig. 3 shows detailed SEM observations of both internal interfaces in Fig. 2. The white top layer in these figures has a thickness up to 20 µm and contains inclusions. At high magnification, the layer can be observed to consist of 'stretched' portions of material: a granular structure deformed opposite to the running direction. This morphology is similar to the plate structure usually observed in thermal martensite. Three possible scenarios may explain this preferred granular orientation:

- plastic deformation of the already transformed structure by tangential wheel-rail interaction; this presumes a sufficient elastic/plastic ratchetting capacity. This are however not typical of thermal martensite.
- phase transformation of a previously deformed structure; this presumes that the deformation occurs in the austenitic phase before the start of the martensitic transformation. Plastic deformation of a metastable austenite leads to a refinement of sub-grains and inhomogeneity of martensite lathes; according to Liu et al. the orientation of martensite lathes can only develop at high deformation temperatures (700°C) [12].
- deformation during the martensitic transformation, known as the plasticity of transformation under external stress. Gautier et al. investigated the kinetics of the martensitic transformation under uniaxial tensile loading for eutectoid steel experimentally. They showed that the effect of plastic shear straining during the martensitic transformation leads to a more pronounced plate structure with an orientation that is favorable with respect to the axial strength [13].

Further investigation is needed to determine which of these mechanisms occur in practice.

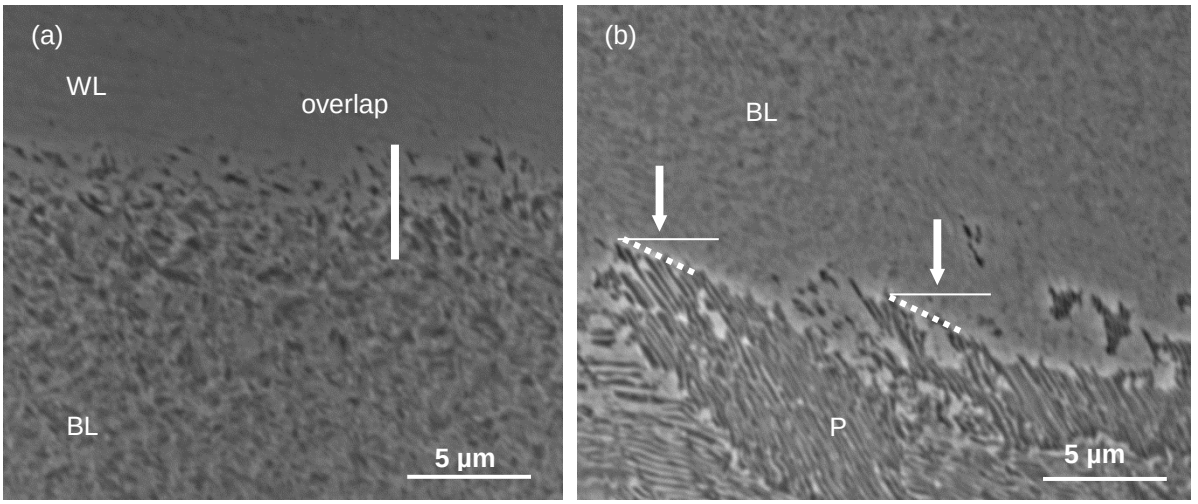

Fig. 3. SEM observations of upper and lower interfaces in stratified layers, (a) white-brown layer transition, (b) brown layer - pearlitic matrix.

Close to the interface with the brown layer, dark 'spots' appear in the white top layer in Fig. 3a. They show that the transition to the brown layer consists of a small zone ('overlap') where the brown phase coexists with the white phase in small embedded 'islands'. This proves a chemical compatibility between the white and the brown layers, implying a strong bonding between the two phases. Within the brown sublayer, a presence of dark 'flocks' can be observed, with a growing intensity toward the upper interface with the white layer. This particular aspect will be discussed later in more detail in paragraph 4.1. No plastic deformation is observed within the brown sublayer.

Fig. 3b shows the transition from the brown layer to the pearlitic parent matrix. The density of the 'flocks' in the structure decreases when approaching the parent matrix, as indicated by the arrows. The bottom of the brown layer is clearly demarcated (as indicated in Fig. 3b); the line segments indicate an abrupt transition between the brown phase and the pearlitic matrix. This is different from the upper interface, which is not a distinct transition. Furthermore, the transition alignment follows a wavy path, which might be explained by grain boundaries.

3. Metallurgical identification of the stratified layer

As discussed in the introduction, the generation of the brown layer has not been extensively studied in the literature. The recent paper by Li et al. [14] gave a detailed description of the brown layer morphology; the fundamental question about the origin and nature of the sublayer remained however open.

Generally speaking, during thermomechanical cyclic contact loading, the occurrence of relatively high temperatures accompanied by excessive shearing in the top layer of the rail may result in phase transformation. Since the findings of the previous section pointed in the direction of a thermal origin of the global layer, it might be assumed that the thermal loading conditions of the pearlitic rail are such that multiple phases are formed apart from martensite. According to the TTT diagram of pearlitic rail grades [15], only the bainitic phase qualifies, and indeed can bainite be formed in a continuous cooling transformation [16]. This hypothesis is formulated and

discussed in more detail in the next chapter; the remainder of this chapter is devoted to the metallurgical identification of the brown etching sublayer, which is helpful in the formulation of the hypothesis.

In order to establish an eventual bainitic phase of the sublayer, different techniques are possible. First of all, the dark appearance of bainite relatively to adjacent martensite under etching with a Nital agent is established in the literature [16]. Under optical microscopy, after etching with Nital, the brown layer exhibits an essentially globular structure with inclusions or islands (see Fig. 2a). This structure is very similar to that of granular bainite as reported in the literature [17,18]. The use of different specific etching agents can however contribute to a more unique determination. Further, hardness measurements can provide useful insight in the microstructural phase composition. Both tests be discussed in the following paragraphs.

3.1. Etching test

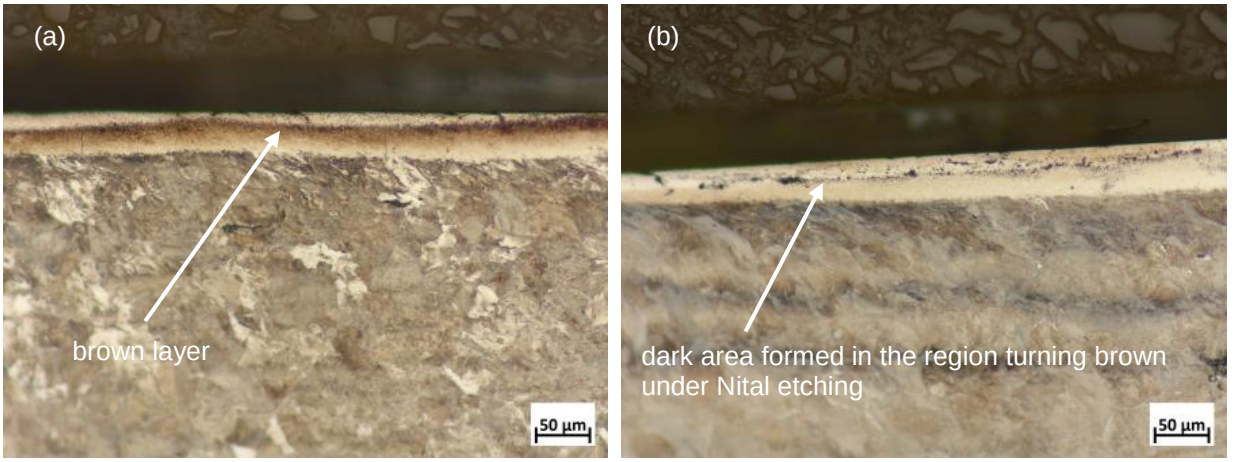

Fig. 4. Illustration of M/A component presence in the brown layer, (a) Nital etching (b) Picric acid etching.

Fig. 4 compares longitudinal cross-sections made from the same specimen of R260Mn, respectively etched with 2 percent Nital and with a Lepera agent which contains a picric acid and sodium picrate [19]. The choice of this agent is based on work by Mazancova [19] and Kremnev [20], according to which granular bainite contains a metallurgical phase reacting with this agent. For Kremnev [20], the bainitic constituent that reacts to the etching is the inclusion that contains retained austenite with globular cementite and ferrite.

In Fig.4b, dark spots are visible that react very strongly to the etching. They occur both within the white top layer and, at a larger scale, in the brown sublayer, the latter clustered along the upper internal interface. This would suggest a presence of inclusions with retained martensite-austenite (M/A).

3.2. Hardness testing

Steel phases can be classified according to their strength and hardness. Microstructural changes and phase transitions inside the stratified layer would therefore induce a changing hardness profile.

Generally, the austenitic phase exists at room temperature in Hadfield manganese steel. This structure has a higher toughness and lower hardness compared to other rail grades such as the pearlitic and bainitic steels [15]. Microstructures with the highest strength result from the austenite-martensite transformation (hardness below 800 Hv); the lowest strength results from the austenite-ferrite transformation. Intermediate strengths are produced by the transformation of austenite to pearlite or bainite; however, bainite exhibits higher hardness as compared to pearlite [21].

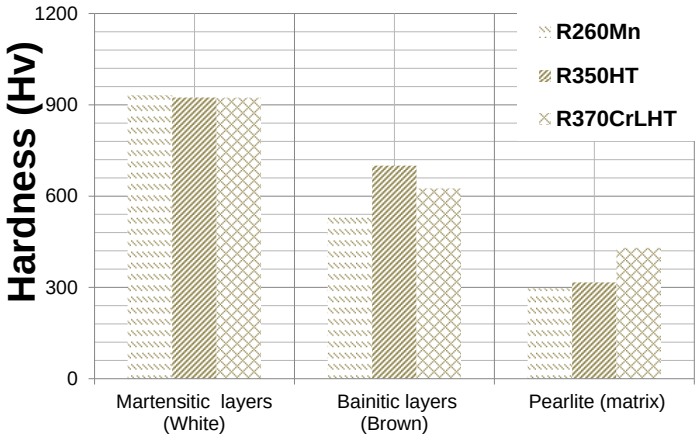

Fig. 5. Hardness comparison of white and brown layers induced by train operation on grades R260Mn, R350HT and R370CrLHT.

Averaged hardness profiles in [6] show that the white top layer has a higher hardness as compared to the brown etching layer, which has on its turn a higher hardness than the parent material, with a local minimum in the darkest brown area, close to the internal interface within the layer. In this study, micro-hardness measurements have been performed on each distinct layer for three pearlitic grades; Fig. 5 depicts the results. All grades, R260Mn, R350HT and R370CrLHT, have been in service for comparable time periods and loading histories. The hardness average obtained within the white layer (martensite) is around 900 HV_{10}, independent from the parent material/rail grade, which therefore seems to have no influence on the martensitic phase. For the brown sublayers, the hardness is reduced as compared to the martensite. A striking difference can however be observed here between the heat treated steels and grade R260Mn. Its background will be discussed in more detail in paragraph 4.3.

4. Hypothesis of stratification generation under wheel-rail loading conditions

This section discusses, in the form of a hypothesis, a mechanism that may lead to the established stratification in the top layer of rails, in line with the observations and properties as established in the first part of the study. The hypothesis incorporates metallurgical and thermomechanical aspects. Metallurgical aspects are discussed separately in the first paragraph. In the next paragraph, the thermomechanical wheel-rail contact conditions are considered in more detail, followed by an integration of both aspects. Paragraph 4.3 discusses further aspects, whereas the last paragraph deals with the spatial arrangement of stratified layers on the railhead in view of the origination hypothesis.

4.1. Metallurgical aspects

According to the earlier cited work by Kremnev [19, 20], granular bainite formation may occur due to supercooling of austenite. A super-cooling transformation is a rapid decrease of temperature accompanied by an incomplete transformation of the austenitic solid solution. The rapid cooling leads to a fluctuation (in time) and redistribution (in space) of the carbon content inside the austenite grain. Consequently, local regions become rich or super-saturated of carbon whereas others become depleted, due to a diffusionless transformation (similar to the martensitic transformation). These carbon fluctuations have an influence on the transformation front between the austenite and the ferrite, becoming a ‘frozen’ interface at the end of the transformation. In fact, this unstable spread of carbon accelerates the generation of ferrite compared to the cementite, and blocks the non-transformed

austenite, appearing in the form of islands or inclusions. Because of the rapid cooling, these islands may transform partially to a martensite-austenite (M/A) constituent; the cementite cannot crystalize as a parallel structure (pearlite) or as disordered lathes (upper or lower bainite), but only in globular form [19, 20].

The granular bainite as described by Kremnev and resulting from supercooling has some striking parallels with the brown sublayer studied in this work, as illustrated in Fig. 6. The dark flocks appearing within the BEL and with the strongest intensity near the interface with the white sublayer (as discussed in chapter 2) can be explained as globular cementite whereas the metallurgical bonding component (clearly visible in Fig. 6 enveloping the dark flocks) is the M/A constituent. In Fig. 4b, this M/A constituent reaches the maximum volumetric fraction at the upper internal interface, appearing in the form of dark clusters.

In chapter 2, the geometry of the BEL-pearlite interface was discussed. The discrete character of the transition can be explained by the spatial blockage of a downward moving phase transformation front; transformation kinetics are stopped because the reaction from austenite to bainitic ferrite cannot occur anymore.

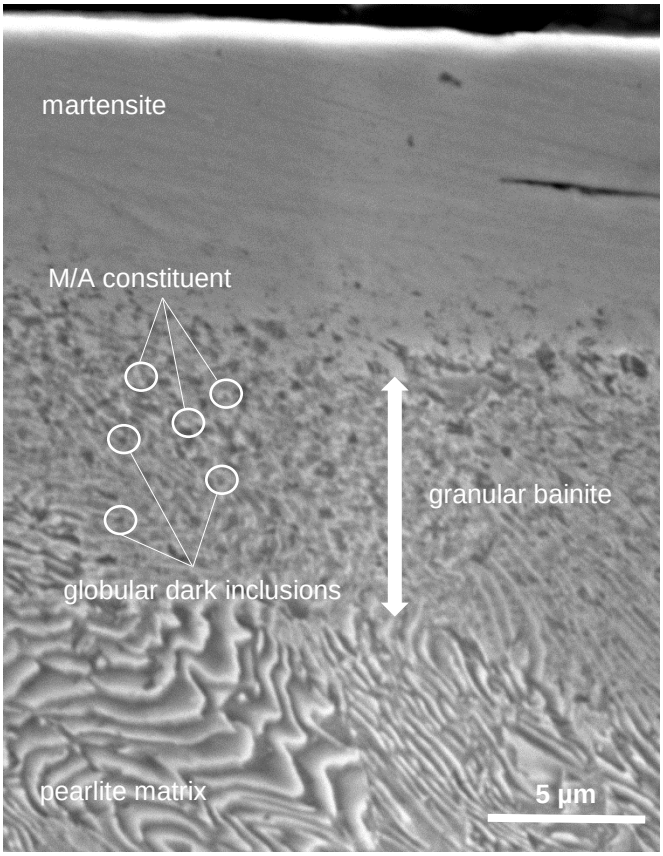

Fig. 6. The stratified layer with metallurgical identification of each layer: martensite, granular bainite with M/A, and pearlite.

It can provide further insight to discuss the eventuality of stratified layer formation (and associated material properties) by purely mechanical wheel-rail interaction, a phenomenon that is known from the literature. Lojkowski describes the distinct top layer resulting from severe plastic deformation as a nanostructured α-Fe–C alloy [22]. This mechanism would allow for the growth of a hardened surface layer at relatively low temperatures. It assumes that the pearlitic cementite dissolves progressively due to the high strains acting on the microstructural inclusions and grain boundaries [23,24]. However, the process of dissolution of cementite, leading from a nodular to a spheroidal appearance in the top layer, is gradual and can never lead to a discrete interface within the top layer itself. Moreover, according to literature, the globular appearance of cementite, even in the case of excessive shear deformation, would require increasing temperatures up to 600 °C [25, 26]. A thermomechanical explanation therefore seems most appropriate for the generation of the morphology of the brown layer.

4.2. Thermomechanical wheel-rail contact conditions

Using a combination of a finite element modelling and building on the analytical approach proposed by Ertz et al.[25], Naeimi et al. [26] studied the spatial contact stress, micro-slip and temperature distribution over the contact patch. They concluded that the flash temperature is related to the micro-slip velocity as a function of the tangential creepage [27], leading to a description of a local thermomechanical cycle as depicted qualitatively in Fig. 7 (p_{max}: maximum contact pressure, τ_{max}: maximum surface shear, T_{max}: maximum temperature).

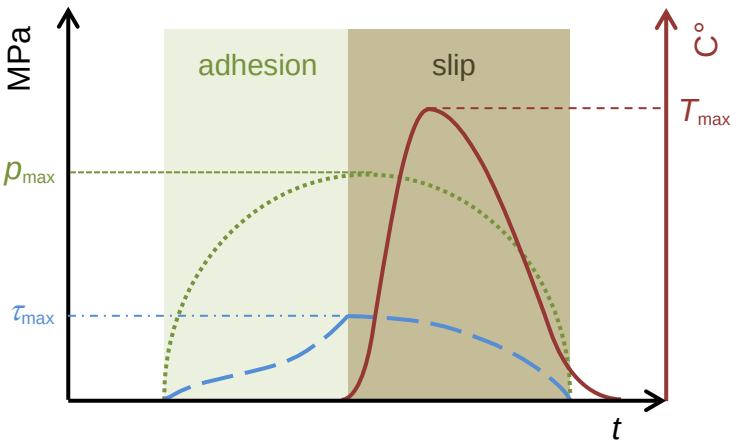

Fig. 7. Qualitative description of a local thermomechanical wheel-rail contact cycle, experienced by a material point on the rail surface, in the time (t) domain.

This figure shows a conceptual thermomechanical cycle that a fixed material point on the rail surface is subjected to under a contact loading cycle in the time domain. The increase in temperature occurs under hydrostatic pressure, with values around 1.8 GPa [8]; it is noted here that Wu et al. suggested that, under similar conditions, the rail composition shifts from the eutectoid to the hypereutectoid and cementite domain in the iron-carbon diagram [8]. The temperature function in Fig. 7 corresponds to the thermal distribution proposed by Bernsteiner et al. [28], who found an increase of temperature in the trailing edge of the wheel-rail contact patch. Besides, they showed that temperatures around the austenitization level are possible. That means at least 700 C° is attained for the R260Mn grade. Their estimation of the maximum temperature showed that values of 1000°C or higher are reachable under extremely severe creepage conditions. They also established that a cyclic wheel-rail loading process induces a repeated deep austenitization (350 -720 µm). The frictional heat in the surface provokes a pearlite-austenite transformation where the temperature exceeds 700 C°, downward into the rail. Bernsteiner et al. assumed that the material over the entire austenized depth transforms into martensite; they validated their assumption using a full-scale simulator with new R260 rail and reproduced an accurate thickness of the white etching layer [28].

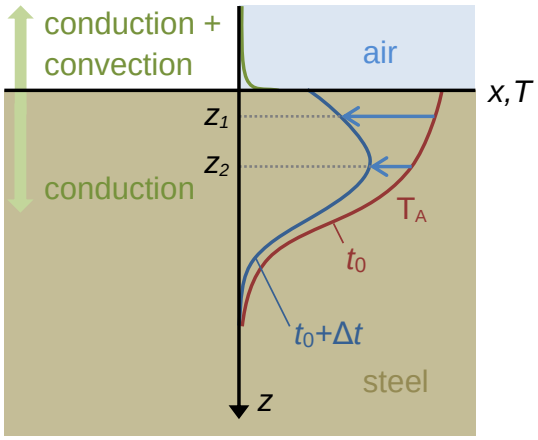

Fig. 8. Qualitative isothermal development/cooling as a function of depth (z) for different time (t) moments after reaching the austenitization temperature T_{AC1} (at time t_0), for a fixed position x_0 along the rail surface: the cooling rate in the subsurface decreases with respect to the surface.

After wheel passage, the thermal energy localised in the heated rail area starts redistributing. A double cooling mechanism occurs at the free surface: conduction and convection (of the relatively cool air). Deeper in the subsurface however, only one mechanism – conduction – can play a role. The effect is, qualitatively, illustrated in Fig. 7. Quantitative simulation of the cooling process in space and time is very difficult, since the convective component depends on the turbulent aerodynamics of the wheel-rail contact, for which there are no models and/or measurements yet available in the scientific literature [25].

From the metallurgical viewpoint, it can be expected that the sudden temperature decrease will start a steel quenching process, causing an immediate martensitic transformation. It can be assumed that the maximum temperature (T_{max} in Fig. 7) is obtained at the surface. Austenitization occurs over a depth with a temperature in the range between the austenitization temperature T_{AC1} and T_{max}. The martensitic transformation takes place when the temperature decreases fast enough below the martensitic start transformation temperature (T_{ms}), which is 200 C° for the R260 grade [28]. When the cooling rate is not fast enough or slowed down for some reason, other phases may be formed according to the Time-Temperature-Transformation (TTT) diagram for the specific steel grade. When the cooling rate, in the line with the previously discussed, becomes essentially depth-dependent, stratification and the formation of different phases becomes a real possibility. The relative difference between cooling rates in the top layer (z_1) and the sublayer (z_2) may then lead to the start of both a martensitic and a bainitic transformation, as illustrated in the conceptual TTT diagram in Fig. 9. The difference in cooling rate as a function of depth can become even more pronounced during the process itself, because martensite is formed first. As a result of the relatively low thermal conductivity of martensite, this will hinder the evacuation of heat in the subsurface [31].

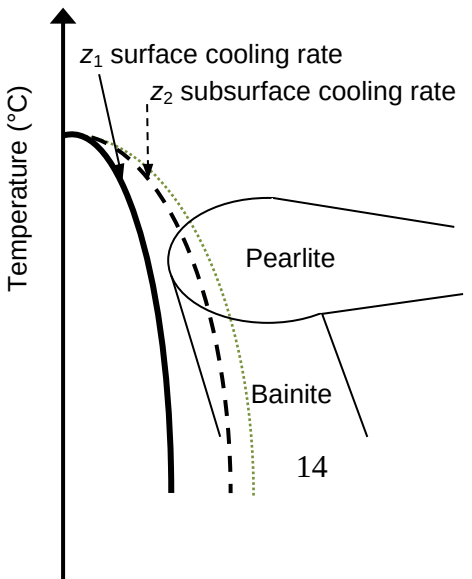

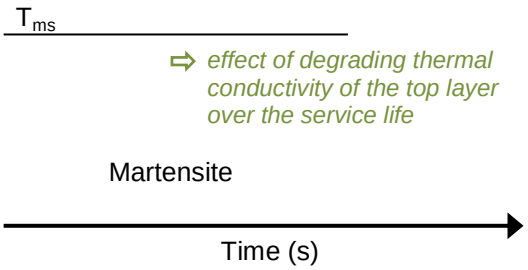

Fig. 9. Representation of an isothermal TTT diagram of pearlitic rail grades [30] [32], cooling rates for positions z_1 and z_2 in Fig. 8, and effect of top layer degradation over the rail service life.

The start temperature of the bainitic transformation (T_{Bs}) can be determined based on the chemical composition of the steel. An empirical equation according to [16,29] is: T_{Bs} (◦C) = 830 − 270W_C − 90W_{Mn} −37W_{Ni} − 70W_{Cr} − 83W_{Mo}. The evaluation of T_{Bs} of both R260Mn and R350HT grades indicates temperatures around 560°C. In accordance to the simulations of Bernsteiner et al. [28], T_{Bs} temperatures are achievable during heating at least 20 µm below the rail surface. Their estimated temperature distributions along with the cooling process as depicted in Figs. 8 and 9 then leads to a stratified phase-transformed surface layer.

4.3. Further discussion

It is straightforward that the total austenitisation depth has a crucial role in the generation of granular bainite, and therefore also with respect to the final geometry of the stratified layer. Fig. 10 shows a comparison between different types of white etching layers. The layer in Fig. 10a is taken from a R260Mn rail that has been in service for only 13 days after fresh milling of the surface. The sample is taken at a specific position in a transverse cross-section over the running band, outside of which this layer does not occur. The ‘fresh’ martensitic layer (consisting of a few ‘lobes’) has a thickness of roughly 15 µm and is not stratified. Moreover, the layer is clearly formed on an undeformed pearlitic matrix; the individual grains and grain boundaries are visible immediately below the interface. The martensitic layer in Fig. 10b (transverse cross-section) is generated by grinding, on the gauge corned of R260 rail. The layer is relatively very thick, about 50 µm, but without any stratification. Also here, there is no plasticity in the subsurface. Fig. 10c shows a longitudinal section over a martensitic WEL on R350HT generated by wheel macroslip (wheel burn) at the edge of the running band. The thickness of the layer is about 40 µm, and again there is no surface plasticity. Fig. 10d shows a transformed surface layer (longitudinal section of

the running band) on a R260Mn rail that has seen 20 MT after maintenance grinding. The total thickness of the layer is about 40 µm and it is clearly stratified. Moreover, in this case plastic deformation is visible both in the white top layer and in the subsurface beneath the brown layer.

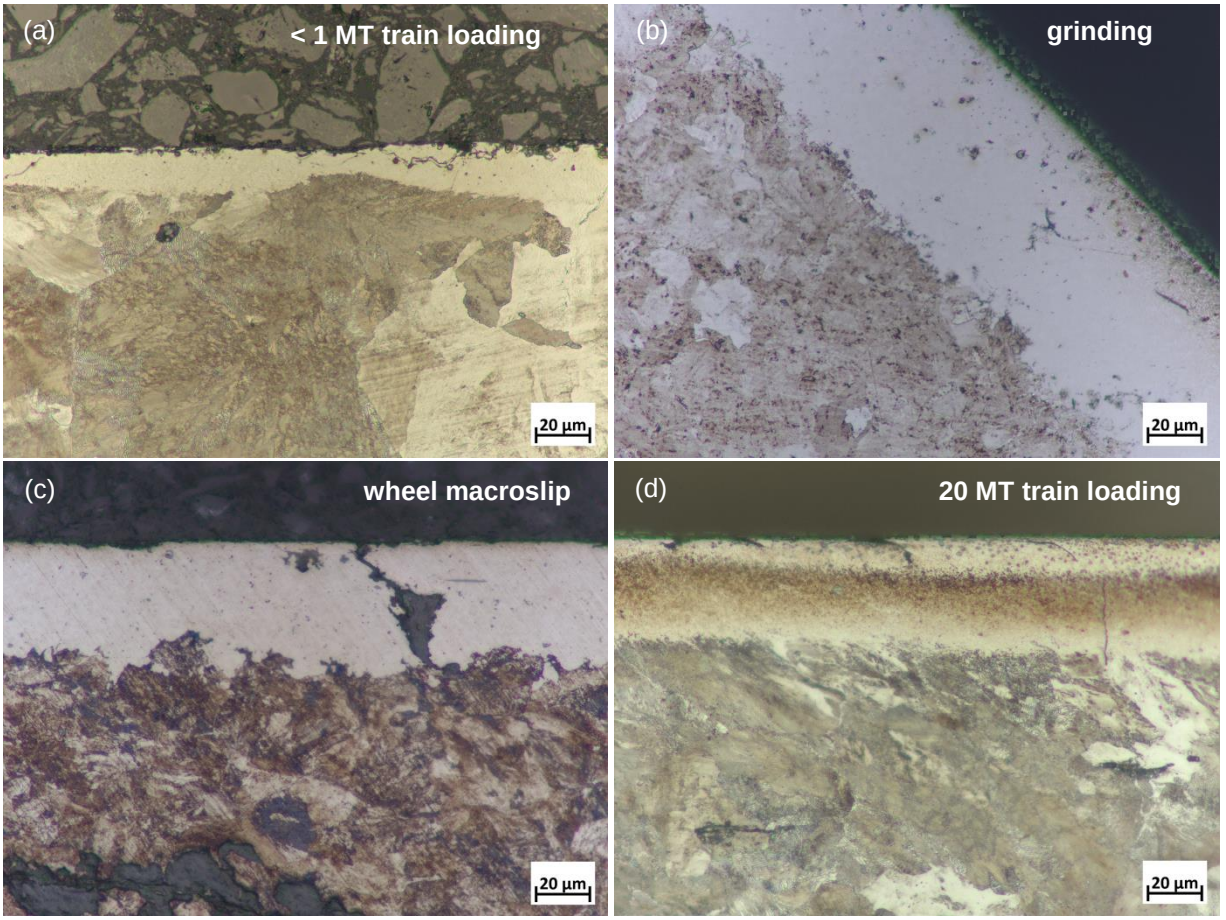

Fig. 10. Comparison of phase-transformed rail surface layers, (a) on R260Mn rail for 13 days in service after milling, (b) on the gauge corner of R260 rail by grinding, (c) on the edge of running band of R350HT due to wheel macroslip, (d) on R260Mn rail after 20 MT borne tonnage.

These examples show that apart from the austenitisation depth and the chemical steel composition, there are still other governing factors with respect to the occurrence of stratification. In the cases depicted in Fig. 10a-c, the cooling rates in the surface and subsurface were high enough to avoid the bainitic domain in the TTT diagram in Fig.9 , whereas for the case depicted in Fig 10d, the subsurface cooling rate was slowed down, for some reason, sufficiently to pass through this domain. The main difference between the samples in Fig. 10 is the borne tonnage at the considered positions; cases a-c have no or almost no contact loading history (and therefore no subsurface plasticity), whereas case d has carried a relatively significant tonnage (accompanied by plasticity). More generally, bainitic sublayers are found frequently on rails that have seen a rather significant tonnage. A further second governing factor with respect to stratification therefore could be the accumulating plasticity and grain

refinement of the top layer under train loading, which is accompanied by a progressive degradation of the thermal conductivity of railhead at a micron and eventually even millimetre scale. Gromov et al. [33] established, in line with common experience, that a long-term operated rail becomes harder over a depth of roughly up to 2 mm. They identified various hardening mechanisms, from which two are similar to high-alloying of steel: the hardening by carbide particles and the hardening by dislocation densification. The thermal conductivity magnitude decreases in the order pure iron - carbon steels - low-alloy steels - high-alloy steels [31], and therefore also a hardened top layer exhibits a reduced thermal conductivity. This can be expected to have an effect notably on the cooling rate of the subsurface, which is achieved only by conduction.

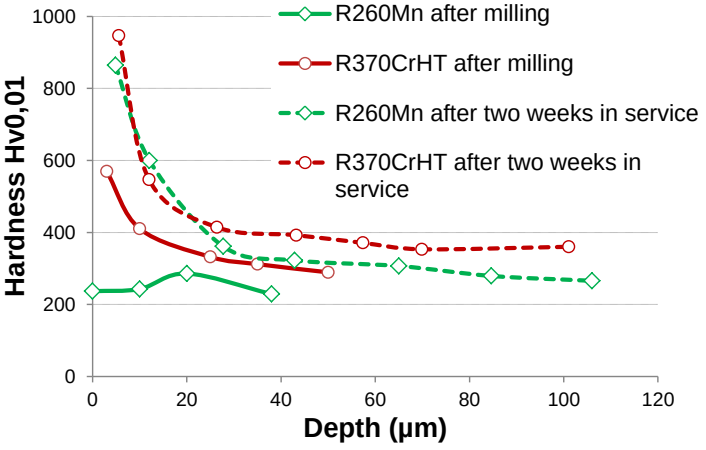

Fig. 11. Hardness development of standard carbon (R260Mn) and premium heat-treated rail (R370CrHT) after identical surface milling, due to a relatively very short period of train loading.

Aging of the rail surface may therefore be expected to increase the susceptibility to bainite formation in a sublayer, as illustrated in the TTT diagram in Fig.9. Moreover, both mentioned hardening mechanisms, consuming carbon atoms, explain the local carbon depletion, promoting the globular inclusions mentioned in paragraph 4.1. Fig. 11 shows the relative hardening of an equally treated surface of both a standard (R260Mn) and premium grade (R370crHT) due to only two weeks of normal train operation. Although both grades tend to achieve similar profiles near the surface independent of the parent material, the difference between the original vs. in-service profiles is much larger for the standard as compared to the premium grade. As many examples in this study show, stratification often involves total layer thicknesses largely exceeding the immediate subsurface (order 50 microns); therefore differences in properties between base/parent and surface material will play a role in the depth-dependent cooling rate. The increased susceptibility of the standard grade, compared to heat-treated

premium grades, to the formation in service of stratified transformed surface layers may therefore be attributed to its increased work hardening capacity.

In chapter 3, it was established that the hardness of the BEL varied significantly with the rail grade. A higher hardness suggests a higher volume fraction of bainite in the case of R350HT and R370CrLHT as compared to R260Mn. This can be explained by the fact that grain refinement leads to higher transformation kinetics and therefore a more 'efficient' transformation into bainite [16]. The hardness variation within the brown sublayer itself can be explained by the fact that the mechanical properties of bulk bainite are strongly dependent on the M/A density [16,34].

The hypothesis in this section about a depth-dependent cooling rate with a higher rate at the surface is corroborated by work in the literature. Ahlström et al. [35] performed numerical simulations with the aim to understand the phase transformations at the wheel surface induced by skidding. They showed that the highest cooling rates are achieved at the free surface of the transformed layer. They also showed that, dependent on the heat exposition time for a given position, multiple phases (including ferrite, pearlite and bainite) would be formed during cooling as expected by the isothermal diagram for the concerned steel grade. This seems in good agreement with their earlier experimental work [36].

4.4. The configuration of stratified surface material within the running band

The spatial arrangement of stratified portions of surface material over the contact surface may provide still further insight concerning its origin. Fig. 12 presents both longitudinal and transversal cross-sections of samples from rails that have been in service. Examples are shown for the three pearlitic grades with similar chemical composition but different grain size: R260Mn (a-d) , R350HT (e, f) and R370CrLHT (g, h). The longitudinal cross-sections for all grades (Figs.12a, e and g) look very similar under optical microscopy, with a white martensitic top layer and a brown bainitic sub-layer. When analysing stratified layers, it can be often remarked that their longitudinal cross-sections show relatively elongated, layered zones with mostly parallel interfaces. This parallel appearance of both layers results from the uniform progress of the spatial austenization-cooling cycle under the moving wheel.

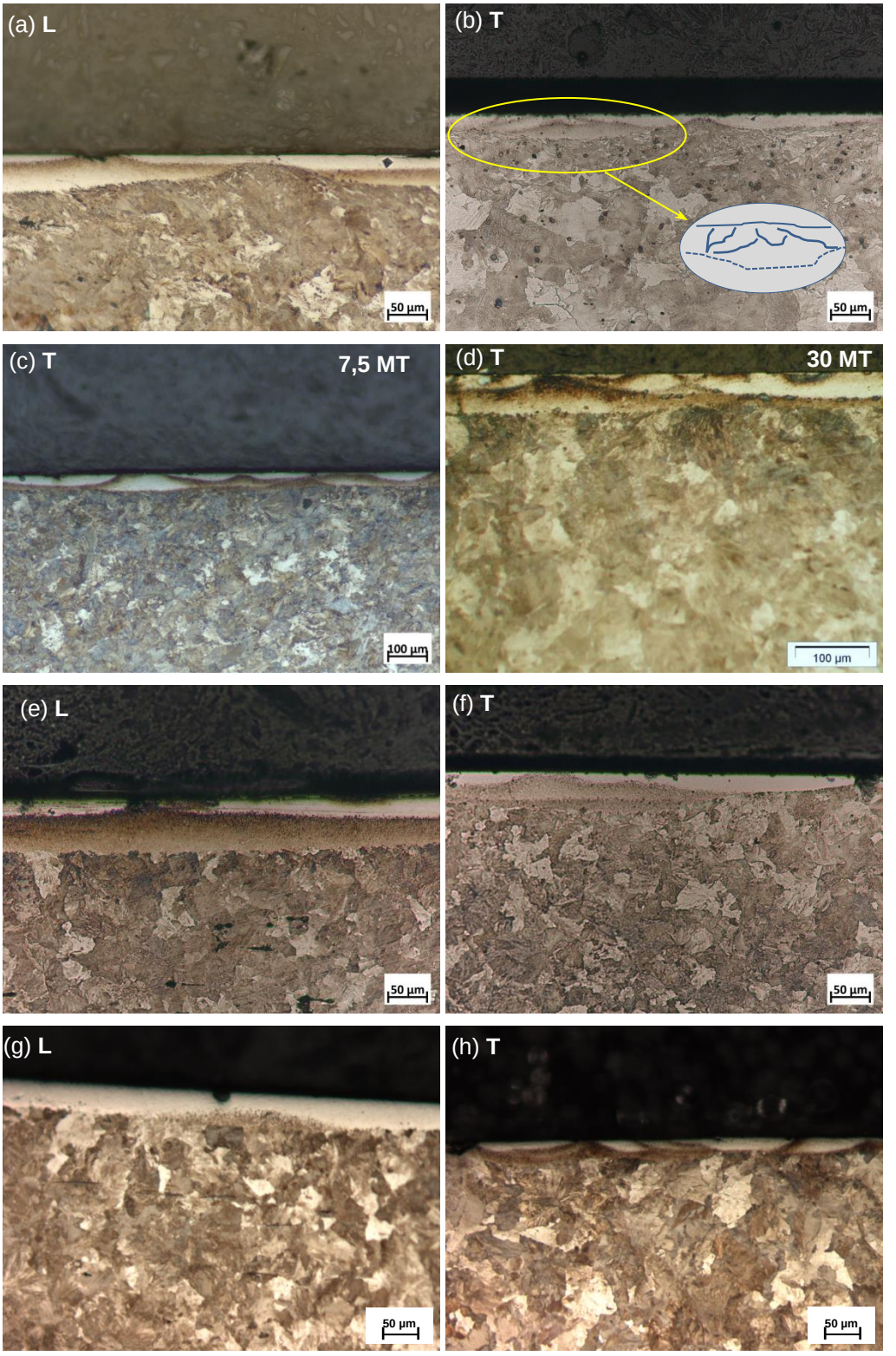

Fig. 12. Longitudinal (L) and transversal (T) cross-sections of stratified layers generated on both R260Mn (a-d), R350HT (e,f) and R370CrHT (g,h).

When observing the transversal sections (Figs. 12b, c, d, f and h) for the three rail grades, they also have the same global topology. The layers are not elongated in this direction but typically have a form that can also be observed, on a macro-scale, in transverse cross-sections of rail repair welding: different ‘lobes’ are visible that partially also overlap. This results in a wavy martensite–bainite interface. Each ‘lobe’ can be assumed to correspond to one single thermomechanical cycle causing phase transformation at that specific location; a cumulated pattern is caused in this sense by different ‘paths’ of the moving wheel-rail contact patch along the surface. Figs. 10c and d shows transverse cross-sections over the running band of the same rail, from tangent track, at two different moments in the loading history: in Fig. 12c, 7.5 MT have passed, whereas in Fig. 12d 30 MT have passed since the latest maintenance grinding cycle (with a nominal take-off of 0,18 mm); the development of the stratified layer is clearly visible with multiple overlaps and a growth in total thickness from 40 to 60 µm.

5. Stratified layers & failure mechanisms

The presence of portions of stratified surface layers on the rail can have an important effect on the RCF resistance and therefore the rail lifecycle. In fact, stratified layers may develop their own failure mechanisms. Fig. 13a and b present observations of damaged stratified layers on grade R260Mn; Fig. 13c, d, e and f show details at higher magnification. Basically, three damage types can be distinguished:

- transverse fracture of either the sandwich layer or the individual bainitic sublayer;
- cracks initiating at an interface, either the martensite-bainite or the martensite-pearlite interface, functioning as a stress raiser;
- inclined crack initiations at the free surface in the white part, clearly influenced by the tangential contact stress history and its directivity.

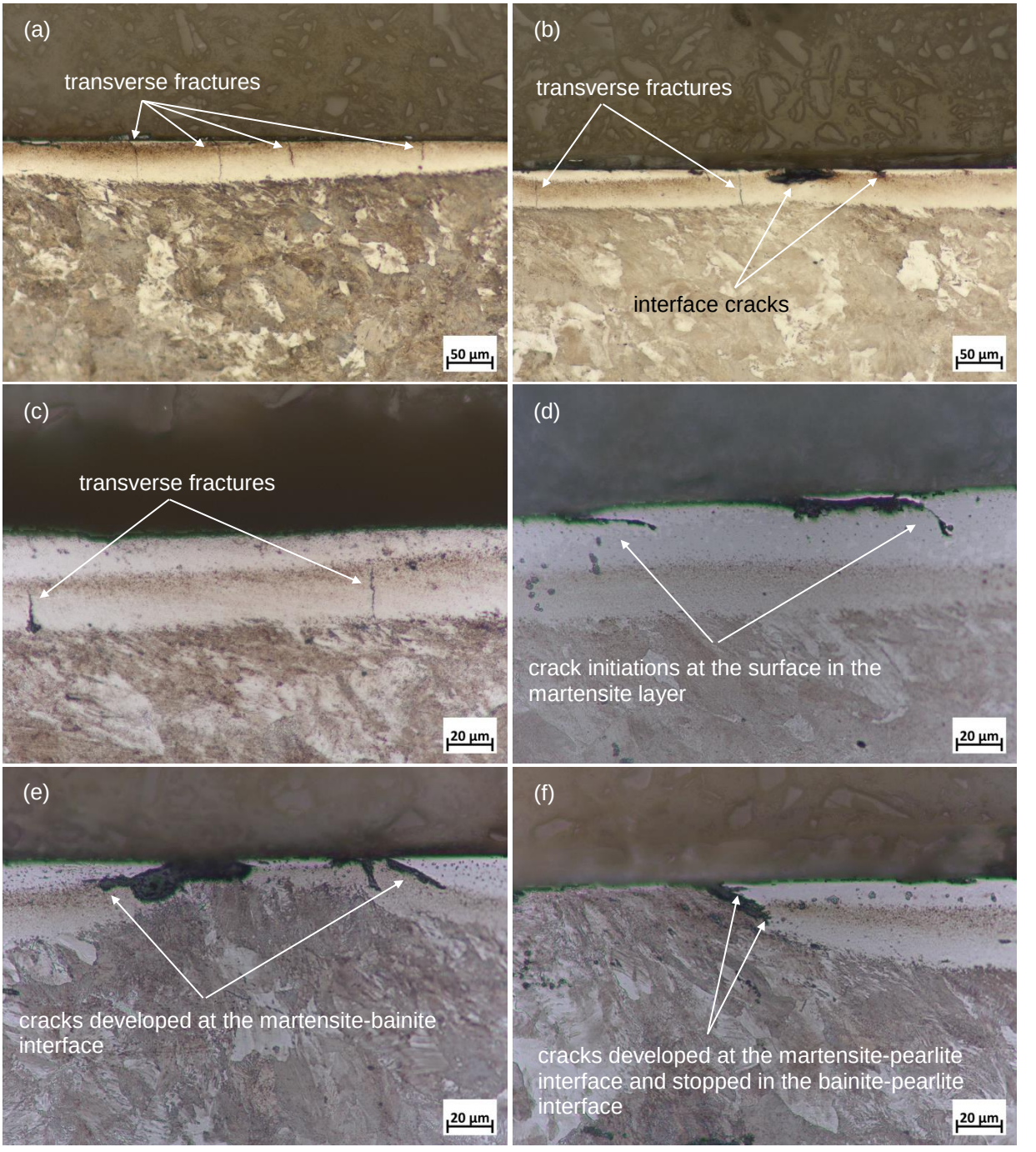

Fig. 13. Longitudinal cross-sections of R260Mn rail developing various failure modes in the stratified surface layer.

Especially the first case is interesting, since it appears that the sublayer may fail individually. It is therefore examined in greater detail. Fig. 14 shows three different cases of transverse fracture of a layer; these cases are analysed with SEM in Fig. 15. Fig. 15a presents a singular crack, exclusively present in the bainitic sublayer and

developed within this phase. Detailed analysis shows that a sequence (“chain”) of globular inclusions (indicated as points) has led to the propagation of the crack through the bainitic matrix.

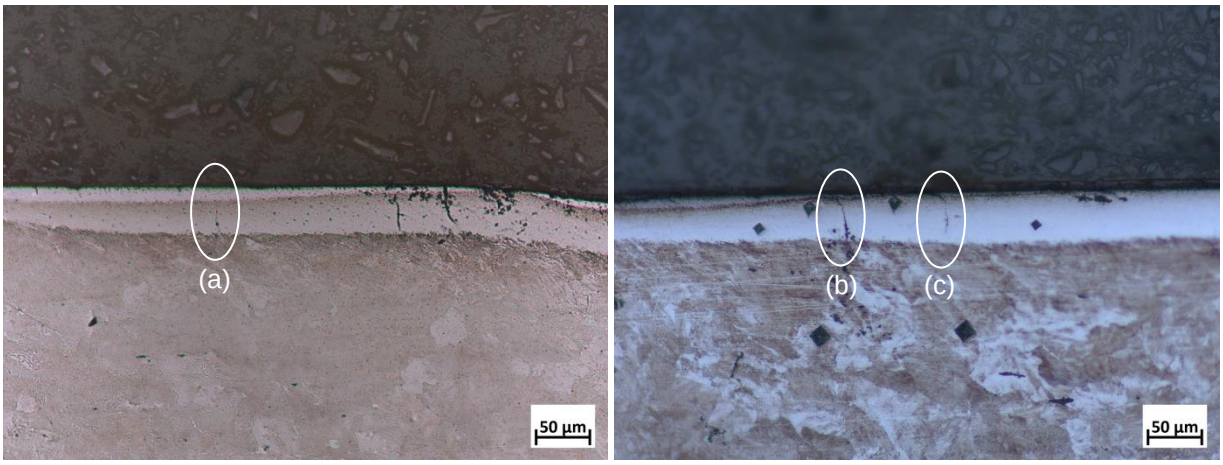

Fig. 14. Transverse fracture of surface layers on R260Mn (longitudinal section).

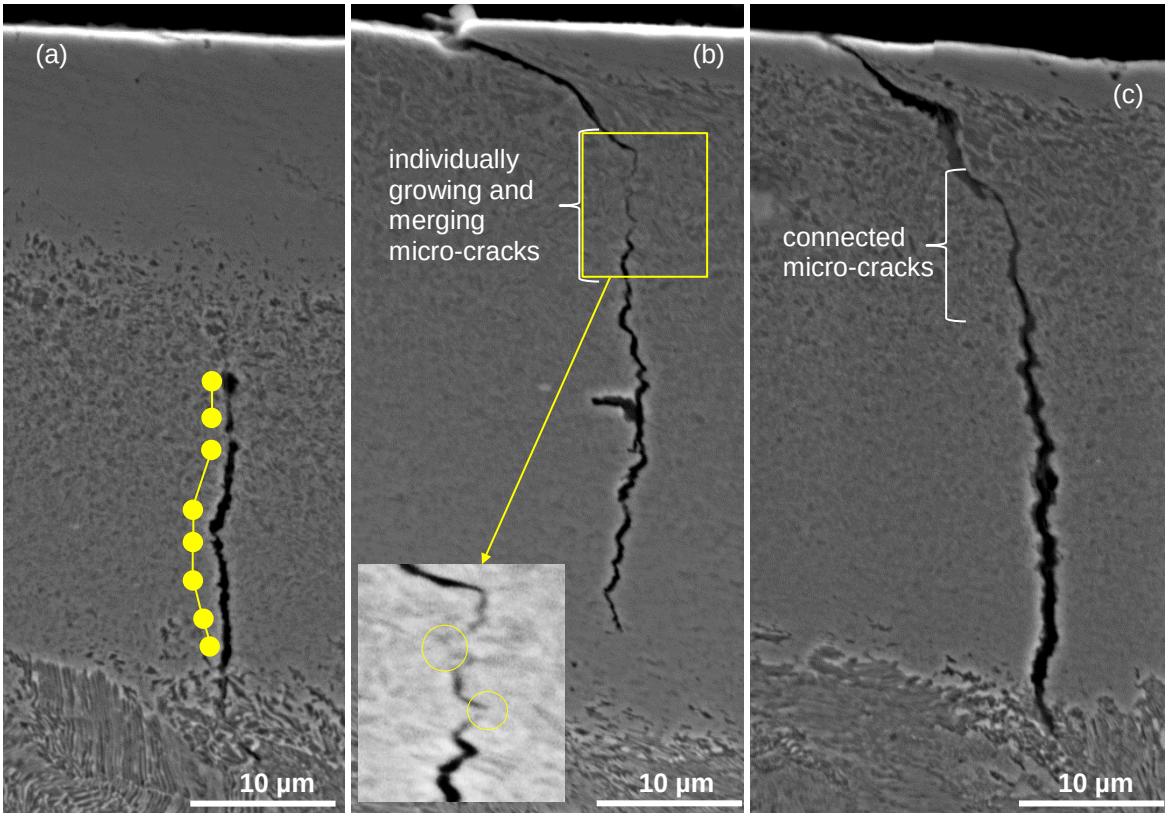

Fig. 15. SEM images of fracture of bainitic sublayers shown in Fig. 13; (a) crack initiation and propagation inside the bainitic structure, (b) crack formation in martensitic and bainitic phases separately, (c) fully developed fracture over the entire sandwich layer, developed separately in martensitic and bainitic phases.

Apparently, the inclusions act as stress concentrators, facilitating crack growth. Since these weak inclusions are absent both in the top layer and the parent material, the inter-granular crack growth mechanism is stopped at both interfaces [17, 37]. Fig. 15b and c present fractures of the entire sandwich layer. The crack orientation in the top layer and the sublayer is different; the orientation in the top layer seems to be influenced by plasticity whereas this is clearly not the case for the sublayer. In the case of Fig. 15b, the cracks in the martensitic and bainitic layers have developed individually and tend to merge; mutual influence by stress amplification can be expected to have had an influence, but there is not one single crack path. In the case of Fig. 15c, again both layers have developed their own crack path, but here the cracks are fully connected so that the entire stratified layer has failed; the crack path is stopped in the pearlite microstructure. Concluding, it may be stated that the failure mode of sublayers in a stratified layer and that of a single martensitic layer is different: whereas the latter is very susceptible to brittle transverse fracture [38], the bainitic sublayer is, due to its microstructural inhomogeneity, relatively susceptible to crack growth inside this layer.

6. Conclusions

This work examined the occurrence and properties of stratified (sandwich) surface layers on rails and presented a hypothesis explaining their origin. More specifically, the study can be summarized in the following conclusions:

- Brown etching sublayers are found on all grades. It has a pronounced globular granular structure in comparison to the white layer and the pearlitic parent matrix; it is found to consist of M/A constituents and globular cementite inclusions forming a bainitic structure. The interface with the pearlitic parent matrix has a clear spatial demarcation whereas the transition to the white martensitic top layer is more diffuse. Hardness and specific etching tests confirm a bainitic phase of the brown sublayer.
- Wheel-rail contact loading establishes a thermomechanical cycle for a fixed material point on the rail surface, with temperatures that may, depending on the creepage, exceed the austenitisation temperature in the subsurface. A difference in the subsequent surface and subsurface cooling rate, caused by the absence of the convection cooling mechanism for the subsurface, could lead to the generation of two different phases, according to the TTT-diagram of the concerned grade, and stratification. Typically, martensite is formed at the surface in such as case whereas bainite is formed in the subsurface.

- Stratified layers have been found exclusively on rails that have been in service, at least for a non-negligible part of their maintenance cycle. Comparison between the WEL generated by macroslip of a train wheel, by grinding and by different tonnages of axle loading on a fresh surface shows the aging of the rail surface (in terms of plasticity) as a significant factor in the occurrence of stratification.
- The exclusive occurrence of sandwich layers on rails that have been in service could be attributed to the hardening of the top layer in comparison to the parent material, yielding a reduced thermal conductivity.
- The granular morphology of the bainitic sublayer with weak globular inclusions facilitates the initiation and the propagation of cracks. Typically, transverse fractures of brown sublayers have been found. Moreover, the additional interfaces between layers favor crack initiation. Therefore, the existence of these layers contributes to the development of RCF.

The present work is a first step in understanding the interaction between thermal and mechanical mechanisms giving rise to the development of stratified surface layers on rails. Future work will deal in more detail with individual aspects of these conclusions.

7. Acknowledgements

This work received no industrial or governmental funding, but was undertaken for the sake of curiosity by the authors at Delft University of Technology.

References

[1] R.I. Carroll, J.H. Beynon, Rolling contact fatigue of white etching layer. Part 2. Numerical results, Wear. 262 (2007) 1267–1273. doi:10.1016/j.wear.2007.01.002.

[2] R.I. Carroll, J.H. Beynon, Rolling contact fatigue of white etching layer: Part 1. Crack morphology, Wear. 262 (2007) 1253–1266. doi:10.1016/j.wear.2007.01.003.

[3] U. Zerbst, R. Lundén, K.O. Edel, R.A. Smith, Introduction to the damage tolerance behaviour of railway rails - a review, Eng. Fract. Mech. 76 (2009) 2563–2601. doi:10.1016/j.engfracmech.2009.09.003.

[4] M. Steenbergen, Rolling contact fatigue in relation to rail grinding, Wear. 356-357 (2016) 110–121. doi:10.1016/j.wear.2016.03.015.

[5] W. Stadlbauer, W. Loos, E.A. Werner, Tribologically induced changes in the microstructure of rail surfaces, 2nd World Tribol. Congr. 651 (2001) 1–4.

[6] S. Li, J. Wu, R.H. Petrov, Z. Li, R. Dollevoet, J. Sietsma, “Brown etching layer”: A possible new insight into the crack initiation of rolling contact fatigue in rail steels?, Eng. Fail. Anal. 66 (2016) 8–18. doi:10.1016/j.engfailanal.2016.03.019.

[7] M. Schilke, Degradation of Railway Rails from a Materials Point of View, 2013.

[8] J. Wu, R.H. Petrov, M. Naeimi, Z. Li, R. Dollevoet, J. Sietsma, Laboratory simulation of martensite formation of white etching layer in rail steel, Int. J. Fatigue. 91 (2016) 11–20. doi:10.1016/j.ijfatigue.2016.05.016.

[9] J. Ahlström, Residual stresses generated by repeated local heating events – Modelling of possible mechanisms for crack initiation, Wear. 366-367 (2016) 180–187. doi:10.1016/j.wear.2016.05.029.

[10] G. Baumann, H.J. Fecht, S. Liebelt, Formation of white-etching layers on rail treads, Wear. 191 (1996) 133–140. doi:10.1016/0043-1648(95)06733-7.

[11] K. Ryttberg, M.K. Wedel, L. Nyborg, Electron microscopy of white-etching band generated by high-velocity parting-off of 100CrMn6 steel, Mater. Sci. Eng. A. 480 (2008) 489–495. doi:10.1016/j.msea.2007.07.041.

[12] C. Liu, Q. Zhao, Y. Liu, C. Wei, H. Li, Microstructural evolution of high Cr ferrite/martensite steel after deformation in metastable austenite zone, Fusion Eng. Des. (2017) 3–7. doi:10.1016/j.fusengdes.2017.03.094.

[13] E. Gautier, J. Zhang, X. Zhang, Martensitic Transformation under Stress in Ferrous Alloys. Mechanical Behaviour and Resulting Morphologies, J. Phys. IV. 5 (1995) 41. doi:10.1051/jp4:1995805>.

[14] Z.D. Li, G. Miyamoto, Z.G. Yang, T. Furuhara, Kinetics of reverse transformation from pearlite to austenite in an Fe-0.6 mass pct C alloy and the effects of alloying elements, Metall. Mater. Trans. A Phys. Metall. Mater. Sci. 42 (2011) 1586–1596. doi:10.1007/s11661-010-0560-4.

[15] J.E. Garnham, C.L. Davis, Rail materials, in R. Lewis, U.Olofsson (Eds), Wheel-Rail interface Handbook , Woodhead Publishing Limited, Cambridge, 2009, pp125-171 . doi:10.1533/9781845696788.1.125.

[16] H. Bhadeshia, R. Honeycombe, Bainite, in H. Bhadeshia, R. Honeycombe, Steels: Microstructure and properties, Fourth ed., Butterworth-Heinemann, Oxford , 2017, pp 179-202. doi:10.1016/B978-0-08-100270-4.00006-8.

[17] F.H. Samuel, D. Daniel, O. Sudre, Further investigations on the microstructure and mechanical behaviour of granular bainite in a high strength, low alloy steel: Comparison of ferrite-pearlite and ferrite-martensite microstructures, Mater. Sci. Eng. 92 (1987) 43–62. doi:10.1016/0025-5416(87)90155-8.

[18] T. Jiang, H. Liu, J. Sun, S. Guo, Y. Liu, Effect of austenite grain size on transformation of nanobainite and its mechanical properties, Mater. Sci. Eng. A. 666 (2016) 207–213. doi:10.1016/j.msea.2016.04.041.

[19] E. Mazancová, K. Mazanec, Physical metallurgy characteristics of the M/A constituent formation in granular bainite, J. Mater. Process. Technol. 64 (1997) 287–292. doi:10.1016/S0924-0136(96)02578-2.

[20] D.P.C. Kremnev, L S, V.V. Svishchenko, Structure and mechanism of the formation of granular bainite in steel 20Kh2NACh, Met. Sci. Heat Treat. 39 (1998) 367–370.

[21] G. Krauss, Strengthening Mechanisms in Steels, Encycl. Mater. Sci. Technol. 20043555 (2001) 8870–8881. doi:10.1201/9780849337987.ch15.

[22] W. Lojkowski, M. Djahanbakhsh, G. Bu, Nanostructure formation on the surface of railway tracks, Mater. Sci. Eng. 303 (2001) 197–208.

[23] F. Wetscher, R. Stock, R. Pippan, Changes in the mechanical properties of a pearlitic steel due to large shear deformation, Mater. Sci. Eng. A. 445-446 (2007) 237–243. doi:10.1016/j.msea.2006.09.026.

[24] T. He, Y. Xiong, F. Ren, Z. Guo, A.A. Volinsky, Microstructure of ultra-fine-grained high carbon steel prepared by equal channel angular pressing, Mater. Sci. Eng. A. 535 (2012) 306–310. doi:10.1016/j.msea.2011.12.091.

[25] M. Ertz, K. Knothe, A comparison of analytical and numerical methods for the calculation of temperatures in wheel/rail contact, Wear. 253 (2002) 498–508. doi:10.1016/S0043-1648(02)00120-5.

[26] M. Naeimi, Z. Li, R. Dollevoet, J. Wu, R.H. Petrov, J. Sietsma, Computation of the flash-temperature at the wheel-rail contact using a 3D finite element model and its comparison with analytical methods, in: 10th Int. Conf. Contact Mech., Colorado, USA, 2015.

[27] M. Naeimi, S. Li, Z. Li, J. Wu, R.H. Petrov, J. Sietsma, R. Dollevoet, Tribology International Thermomechanical analysis of the wheel-rail contact using a coupled modelling procedure, Tribol. Int. 117 (2018) 250–260. doi:10.1016/j.triboint.2017.09.010.

[28] C. Bernsteiner, G. Müller, A. Meierhofer, K. Six, D. Künstner, P. Dietmaier, Development of white etching layers on rails: simulations and experiments, Wear. (2016) 1–7. doi:10.1016/j.wear.2016.03.028.

[29] H. Bhadeshia, R. Honeycombe, Heat Treatment of Steels: Hardenability,in in H. Bhadeshia, R. Honeycombe, Steels: Microstructure and properties, Fourth ed., Butterworth-Heinemann, Oxford , 2017, pp 217-236. doi:10.1016/B978-0-08-100270-4.00008-1.

[30] A.K. Nath, S. Sarkar, Laser Transformation Hardening of Steel, in Jonathan Lawrence, Advances in Laser Materials Processing, Technology, Research and Applications, Second Edi, Woodhead Publishing, Cambridge, 2018, pp 257-298. doi:10.1016/B978-0-08-101252-9.00011-X.

[31] M.J. Peet, H.S. Hasan, H.K.D.H. Bhadeshia, Prediction of thermal conductivity of steel, Int. J. Heat Mass Transf. 54 (2011) 2602–2608. doi:10.1016/j.ijheatmasstransfer.2011.01.025.

[32] F. Fau, Personal communication with authors, British Steel, 2017.

[33] V.E. Gromov, Y.F. Ivanov, O.A. Peregudov, K.V. Morozov, X.L. Wang, W.B. Dai, Y.V. Ponomareva, O.A. Semina, Evolution of structure and properties of railhead fillet in long-term operation, Mater. Electron. Eng. 2 (2015) 2–5. doi:10.11605/mee-2-4.

[34] F.G. Caballero, H.K.D.H. Bhadeshia, K.J.A. Mawella, D.G. Jones, P. Brown, Very strong low temperature bainite Very strong low temperature bainite, Mater. Sci. Technol. 18 (2002) 279–284. doi:10.1179/026708301225000725.

[35] J. Ahlström, B. Karlsson, Modelling of heat conduction and phase transformations during sliding of railway wheels, Wear. 253 (2002) 291–300.

[36] J. Ahlström, B. Karlsson, Microstructural evaluation and interpretation of the mechanically and thermally affected zone under railway wheel flats, Wear. 232 (1999) 1–14.

[37] C. Kammerhofer, a. Hohenwarter, S. Scheriau, H.P. Brantner, R. Pippan, Influence of morphology and structural size on the fracture behavior of a nanostructured pearlitic steel, Mater. Sci. Eng. A. 585 (2013) 190–196. doi:10.1016/j.msea.2013.07.032.

[38] M. Steenbergen, R. Dollevoet, On the mechanism of squat formation on train rails - Part I: Origination, Int. J. Fatigue. 47 (2013) 361–372. doi:10.1016/j.ijfatigue.2012.04.023.